RESEARCH PAPER

Synthesis and characterization of carbon-covered alumina (CCA) supported TiO$_2$ nanocatalysts with enhanced visible light photodegradation of Rhodamine B

**Mphilisi M. Mahlambi · Ajay K. Mishra ·
Shivani B. Mishra · Rui W. Krause ·
Bhekie B. Mamba · Ashok M. Raichur**

Abstract The anatase phase of titania (TiO$_2$) nano-photocatalysts was prepared using a modified sol gel process and thereafter embedded on carbon-covered alumina supports. The carbon-covered alumina (CCA) supports were prepared via the adsorption of toluene 2,4-diisocyanate (TDI) on the surface of the alumina. TDI was used as the carbon source for the first time for the carbon-covered alumina support system. The adsorption of TDI on alumina is irreversible; hence, the resulting organic moiety can undergo pyrolysis at high temperatures resulting in the formation of a carbon coating on the surface of the alumina. The TiO$_2$ catalysts were impregnated on the CCA supports. X-ray diffraction analysis indicated that the carbon deposited on the alumina was not crystalline and also showed the successful impregnation of TiO$_2$ on the CCA supports. In the Raman spectra, it could be deduced that the carbon was rather a conjugated olefinic or polycyclic hydrocarbons which can be considered as molecular units of a graphitic plane. The Raman analysis of the catalysed CCAs showed the presence of both the anatase titania and D and G band associated with the carbon of the CCAs. The scanning electron microscope micrographs indicated that the alumina was coated by a carbon layer and the energy dispersive X-ray spectra showed the presence of Al, O and C in the CCA samples, with the addition of Ti for the catalyst impregnated supports. The Brunauer Emmet and Teller surface area analysis showed that the incorporating of carbon on the alumina surface resulted in an increase in surface area, while the impregnation with TiO$_2$ resulted in a further increase in surface area. However, a decrease in the pore volume and diameter was observed. The photocatalytic activity of the nanocatalysts was studied for the degradation of Rhodamine B dye. The CCA-TiO$_2$ nanocatalysts were found to be more photocatalytically active under both visible and UV light irradiation compared to the free TIO$_2$ nanocatalysts.

M. M. Mahlambi · A. K. Mishra (✉) ·
S. B. Mishra · R. W. Krause · B. B. Mamba
Department of Chemical Technology, University of Johannesburg, P.O. Box 17011, Doornfontein 2028, South Africa
e-mail: amishra@uj.ac.za

A. M. Raichur
Department of Materials Engineering, Indian Institute of Science, Bangalore 560012, India

Introduction

Titanium dioxide (TiO$_2$ or titania) is a metal oxide semiconductor that has been extensively studied and

thus as a photocatalyst it has been used in coating self-cleaning surfaces, as environmental purifiers and in antifogging mirrors (Hoffmann et al. 1995; Mori et al. 2008; Foster et al. 2011). Owing to its peculiar and fascinating physicochemical properties, titania is a very important environmental and energy material with a wide variety of potential applications in diverse fields including gas sensors, part of photovoltaic devices, dielectric ceramics and catalysts for thermal or photo induced processes. Its properties which include, among others, long-term stability, non-toxicity, low price and superior photo-reactivity has led to TiO_2 gaining more prominence over most semiconductors (Ahn et al. 2007; Yu et al. 1997; Zhu et al. 2005; Tian et al. 2009; Li et al. 2008; Colmenares et al. 2006; Foglia et al. 2009; Yu and Zhang 2010). Various parameters like crystallinity, impurities, surface area and density of surface reactive sites results in an enhanced photocatalytic activity; however, crystallinity is the most important factor (Fu et al. 2005; Ao et al. 2008). The photocatalytic reactions are initiated when the TiO_2 semiconductor absorbs energy (a photon or hv) resulting in an excitement of an electron from the valence band to the conduction band. Electron can only be excited if the energy of the photon is equal to or exceeds the band gap ($E_{bg} = 3.0$–3.2 eV) of the titania semi-conductor (Hoffmann et al. 1995; Bessekhouad et al. 2003; Zhu et al. 2008). The electron (e^-) and the hole (h^+) act as the redox pair, and separation of these charges is imperative to result in enhanced oxidation and reduction, respectively (Fu et al. 2005; Hoffmann et al. 1995; Wang et al. 2008). The separated two charge carriers (e^- and h^+) therefore propel the photo-electrochemical red-ox reactions with the redox molecules at the semiconductor surface (Bessekhouad et al. 2003; Chen and Mao 2007). However, to increase the photocatalytic activity and recoverability of titania from aqueous media, these catalysts can be embedded on catalysts' supports.

Carbon and alumina are the mostly widely used for support materials. However, their exclusive use as catalysts' supports has some major drawbacks. Alumina, for instance, is an acidic support upon calcination reacts with the promoter ions (e.g. Co and Ni) resulting in the formation of unwanted metal oxides resulting in reduced the catalysts activity (Vissers et al. 1988; Boorman and Chong 1993; Zheng et al. 2008). Carbon supports, on the other hand, are either microporous or have poor mechanical strength and hence are not favourable support materials as they

easily crush and have low bulk density (Boorman and Chong 1993; Błachnio et al. 2007). Also, metals catalysts supported on carbon can be deposited on the micropores of the carbon supports hence making their catalytic activity trivial (Błachnio et al. 2007).

However, both alumina and carbon supports have desirable properties. For instance, alumina supports have the ability to disperse up to 20% of the active metal phase, have high surface area as well as good mechanical properties (Vissers et al. 1988; Zheng et al. 2008). Carbon supports have mild interactions with the supported metals, a neutral surface, good thermal conductivity, high surface area with controlled pore volume, reduced coking propensity, resistance to nitrogen poison and variable surface functional groups which give carbon a tremendous scope for use as catalyst support material (Zheng et al. 2008; Boorman and Chong 1993).

A support is very important for a catalyst since it determines the catalytic activity of the catalyst. However, the exclusive use of carbon or alumina as catalyst supports can result in the loss of the catalytic activity of the catalysts; hence, a support system that exploits the merits of both substances can provide an ideal support system which overcomes the shortcomings of both. In this system, the alumina is coated with a thin layer of carbon before catalyst impregnation resulting in a support material that possesses both the textural and mechanical properties of alumina and the favourable surface properties of carbon (Boorman and Chong 1993; Błachnio et al. 2007; Zheng et al. 2008). The utilisation of these carbon-covered alumina materials as catalyst supports has gained an increasing interest in recent years (Błachnio et al. 2007; Boorman and Chong 1992; Lin et al. 2005a, b; Maity et al. 2009; Polyánszky and Petró 1990; Sharanda et al. 2006; Shashikala et al. 2007; Vissers et al. 1988; Zheng et al. 2008).

Carbon-covered alumina supports have been mostly used as supports for hydrotreating catalysts (Vissers et al. 1988; Boorman and Chong 1992; Maity et al. 2009) and ammonia synthesis (Rao et al. 1990). Recently, supports have found a lot of useful applications. For instance, CCA been used as a high surface area packing material for high performance liquid chromatography (Paek et al. 2010), and has also been prepared in various forms like carbon-coated alumina foams (Jana and Ganesan 2011). CCA-supported catalysts have hardly been used in remediation of

environmental burdens. According to literature, only nano-silver catalyst has been supported on CCA to monitor microorganisms in drinking water (Shashikala et al. 2007). Also, according to our best knowledge, TiO$_2$ nanocatalysts have never been supported on carbon-covered alumina supports. In this research, titania nanoparticles will be supported on CCA supports. This is expected to enhance the visible light photo response of the catalysts and also help to prevent the agglomeration of the nanoparticles when subjected to photocatalytic experiments. Supporting these CCA-supported TiO$_2$ nanocatalysts therefore plays a major part of this research and is expected to pave way for the use of renewable solar energy for environmental photocatalytic processes. The use of nanocatalysts (especially titanium dioxide or titania or TiO$_2$) has gained wide recognition since they have the potential to tackle the 'difficult-to-remove' contaminants and thus are expected to play an important role in solving many serious environmental and pollution problems. Titania catalysts not only show excellent catalytic performance with some of the highest selectivities known in the literature so far, but also its lower price in comparison to other catalysts increases its attractiveness as catalyst for use in environmental applications (Ulgen and Hoelderich 2011; Calandra et al. 2010). Also, the controllable synthesis of anatase titanium dioxide is another add-on to the wide investigation of TiO$_2$ for important industrial and environmental applications (Fang et al. 2011). In this study, we report on the synthesis and characterizations of the physical and textural properties of nano anatase TiO$_2$ catalysts supported on carbon-covered alumina.

Experimental

Materials and methods

Titanium (IV) tetraisopropoxide (TTIP) (99%) was obtained from Sigma-Aldrich (Germany) and used without further purification. Formic acid (98%) was purchased at Merck and AR grade n-propanol was sourced from SD's Fine Chem (Pty) Ltd., and was distilled before usage. γ-Alumina was purchased from Sigma-Aldrich and was calcined at 500 °C for 3 h in a muffle furnace to remove any organic impurities that might have been present. Toluene 2,4-diisocyanate was supplied by Industrial Polyurethanes (Edenvale,

South Africa) and was used without purification. n-Xylene (AR grade) was purchased from Sigma-Aldrich and was dried on calcium hydride fro 24 h before usage.

Synthesis of catalysts and supports

Synthesis of TiO$_2$ nanocrystalline photocatalysts

For the synthesis of the anatase rich titania nanocatalysts, TTIP was hydrolysed through an esterification reaction between formic acid and propanol (Zhu et al. 2005) TTIP (10 mL, 0.334 mol) was dissolved in propanol (48 mL, 0.642 mol) and the reaction mixture was stirred for 20 min. Formic acid (13 mL, 0.535 mol) was gradually added while stirring gently. After stirring the reaction mixture for about 20 min, a white precipitate (titanium hydroxide) was gradually formed. This mixture was then stirred for a further 2-h period, aged at room temperature for another 2 h and filtered. The filtered residue was then repeatedly washed with copious amounts of propanol and deionized water; thereafter it was dried overnight in an oven at 80 °C. It was then ground into fine powder in a mortar and pestle and then calcined at 450 °C to obtain nanocrystalline TiO$_2$ catalysts.

Synthesis of carbon-covered alumina supports

CCA supports were synthesized by modification of an equilibrium adsorption method by Sharanda et al. (2006). A mixture of γ-alumina (5 g) and 1% TDI in n-xylene (115 mL) was occasionally shaken for 24 h at room temperature. The reaction mixture was filtered and washed with n-xylene (100 mL). A white fluffy precipitate was obtained. This was dried in an oven at 80 °C overnight. The obtained precipitate was then ground in a pestle and mortar and placed into a quartz cell. The temperature was slowly increased to 700 °C under 30 mL min^{-1} flow of nitrogen and the temperature was held at that temperature for 3 h in order to complete the pyrolysis of TDI and remove volatile products.

Impregnation experiments

To impregnate the CCA supports with the nanocatalysts, TiO$_2$ nanocatalysts were dissolved in distilled water to form a colloidal suspension. These were sonicated for 30 min at room temperature. CCA

supports were then added on the TiO_2 suspensions. The impregnated CCA supports were then sonicated for 1 h and left at room temperature for 24 h to dry. These were further dried in an oven at 80 °C for 12 h (overnight). After drying, these were then ground in a pestle and mortar and calcined at 450 °C for 3 h in a muffle furnace to afford the TiO_2-impregnated CCA supports.

Characterization

XRD spectroscopy analysis

The XRD measurements were carried out using an X'Pert Pro MPD PANalytical powder diffractometer operating in the reflection mode with CuKα radiation. The XRD chromatograms were recorded over an angular range of 20–80 °C (2θ) and with a step size of 0.02° and a collection time of 0.3 s ($\lambda = 0.154060$ nm). A shape factor K is used in X-ray diffraction and crystallography to correlate the size of sub-micrometer particles, or crystallites. The Debye–Scherrer equation, $D = K\lambda/B \cos \theta$, was used to correlate the particle size, where the constant $K = 0.89$, $\lambda = 0.154060$ nm is the X-ray wavelength, B is the full width half maximum (FWHM) of the catalyst, and θ is the diffracting angle. The JCPDS XRD library software was used to confirm the Miller planes of the CCA supports.

Raman spectroscopy

For Raman analysis, a PerkinElmer Raman Micro 200 was used. This was equipped with a laser lamp operating at a wavelength of 785 nm and had a maximum output of 250 mW. For analysis, the sample was placed on a quartz slide on the stage of the microscope and the focus was adjusted manually to obtain the best image. This was then switched to the dark field and the beam was passed on the sample to record the spectrum.

SEM, TEM and EDX spectroscopy

A quanta FEI-SIRION SEM was used to analyse and visualise the surface morphology of the nanocatalysts. The powder samples were placed on a carbon tape and analysed without gold coating. A JEOL J2100 F TEM was used to study the microstructure of the nanocatalysts. The sample powders were dispersed in ethanol and sonicated for 10 min before analysis. A drop of the suspension was then placed on a carbon-coated copper grid and dried in air before visualisation. Both the SEM and TEM were coupled with an EDX detector, which was used to determine the identity of the alumina, the free carbon-covered alumina and the TiO_2-impregnated carbon-covered alumina supports.

BET surface area and pore size distribution measurements

To study the surface area (S_{BET}), pore volume and pore size distributions of the synthesized CCA supports, a Micromeritics ASAP 2020 Surface area and Porosity Analyzer was used. The samples were degassed in nitrogen under vacuum for 24 h at 200 °C before determination of the surface area. Typically, the samples were heated to 90 °C at a heating rate of 5 °C min^{-1} and the temperature was held at 90 °C for 180 min. The samples were then evacuated at a pressure of 50 mmHg for 30 min. The samples were then ramped to 180 °C at a heating rate of 10° min^{-1} and degassed for 24 h under nitrogen. Surface area is believed to be an important parameter when studying the catalytic efficiency of the nanocatalysts embedded on CCA supports (CCA-TiO_2) since a high surface area means more active sites for extensive catalysis.

Photocatalytic degradation studies

A Newport 9600 Full Spectrum Solar Simulator equipped with 150 W ozone free xenon lamp which produces a collimated beam of 33-mm diameter, an equivalent of 1.3 suns was used to study the degradation Rhodamine B by the titania photocatalysts. The distance between the solar simulator and the experimental set up was set such that the beam power was equivalent to 1 sun (about 10 cm). A high-pressure 125 W mercury vapour lamp (Samson, India) was used as the UV irradiation source. The photocatalytic activity of these nanophotocatalysts was studied using 100 mL (10 mg L^{-1}) Rhodamine B. The CCA-supported titania nanoparticles (100 mg nanoparticles per 100 mL of 10 mg L^{-1} dye) were used in suspension to determine the photoactivity of the nanoparticles. The solution was stirred with a magnetic stirrer for 1 h before irradiation with the solar light to establish an

adsorption–desorption equilibrium between the dye and the catalyst surface. Aliquots of 2 mL were extracted from the reaction chamber at 30-min intervals to study the extent of the degradation. The entire photo reactor setup was set inside a 100 cm × 70 cm wooden box. The set up was the same for the free (unsupported) titania nanocatalysts.

Results and discussions

XRD spectroscopy analysis

From the XRD patterns (Fig. 1), the CCA supports (A) do not show peaks associated with carbon and this means that characterisation of the CCAs with XRD did not reveal any peaks associated with the ordered carbon structures (Sharanda et al. 2006). The only peaks that could be seen are those associated with the alumina at $2\theta = 37.5$ (311), 39.5 (222), 42.9 (321) 45.6 (400) and 67.5 (411). These peaks concur with XRD data obtained from the JCPDS library catalogue number 04-0880. This therefore means that the presence of either amorphous carbon layer or a thin graphitic layer can only be assumed due to the black colour observed. Graph (A) shows peaks associated with pure anatase phase. The XRD peaks obtained at calcination temperatures of 450 °C corresponds to the tetragonal anatase titania phase of the titania and this was confirmed by cross referencing with the JCPDS CAS No. 21-1272 (JCPDS catalogue). The peaks that were observed at $2\theta = 25.2$ (101), $2\theta = 37.9$ (004),

$2\theta = 48.0$ (200), $2\theta = 53.9$ (106) and $2\theta = 62.7$ (215) indicate the successful synthesis of the anatase phase of TiO_2. The peaks $2\theta = 27.5$ (a rutile-phase peak) due to the (110) reflection and $2\theta = 30.8$ (121) which is a brookite phase, and this is an indication of the absence of these phases in our synthesized titania (Navio et al. 1999; Anandan et al. 2008). Graph (B), which is of the TiO2-embedded CCA supports exhibit both the peaks associated with TiO_2 and CCA. This is an indication that embedding the TiO_2 nanocatalysts on the CCAs did not alter the core of the titania phase (anatase) or the CCA supports.

Raman spectroscopy

The UV Raman spectrum of the CCA supports is shown in Fig. 2 (insert). Two peaks that were assigned to the D and G bands were observed at 1318 and 1607 cm^{-1}, respectively, and are due to the sp^2 carbon species (Zheng et al. 2008; Lin et al. 2005b). These two peaks are common for various forms of disordered, noncrystalline and amorphous carbons observed in the Raman spectra. The D (disorder) band is related to the breathing modes of the sp^2 carbon atoms in the ring, while the G band is due to bond stretching of the sp^2 carbon atoms. The widths, dispersions and intensities of these peaks are different for various carbons and hence provide powerful information for differentiating carbon species (Lin et al. 2005b). The D peak can be fitted into three peaks which are observed at 1165, 1318 and 1386 cm^{-1}. The G band was observed at
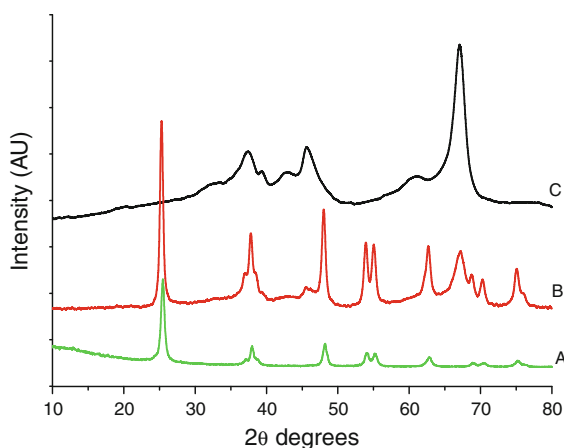

Fig. 1 XRD patterns of TiO_2 (*A*), TiO_2 impregnated CCA (CCA-TiO_2) (*B*) and CCA (*C*)
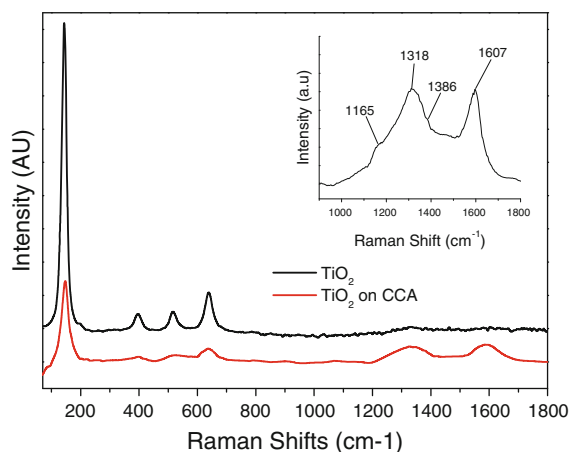

Fig. 2 UV Raman Spectra of the titania impregnated CCA supports

1607 cm^{-1}, and this is an indication that the carbon layer on the CCAs was possibly related to conjugate olefinic species or polycyclic aromatic hydrocarbons. This peak usually appears at lower wavelengths of 1582 cm^{-1} when the carbon layer is crystalline graphite (Lin et al. 2005b). This means that the carbon layer deposited on the alumina surface is not crystalline. It is therefore reasonable to speculate that the Raman analysis explains why there are no carbon peaks observed on the XRD chromatograms.

The Raman spectra of the titania in Fig. 2 show that the titania is anatase phase. The peaks observed are associated with the primitive unit cell of the anatase titania phase. It is tetragonal and has fifteen (15) irreducible optical modes which are represented by $1A_{1g} + 1A_{2u} + 2B_{1g} + 1B_{2u} + 3E_g + 2E_u$. The A_{1g}, B_{1g} and E_g modes are Raman active, while the A_{2u} and E_u are infra red active (Ohsaka et al. 1978). From Fig. 3, the two Raman bands at 516 and 399 cm^{-1} are the B_{1g} stretching modes while the three Raman bands at 639, 197 and 144 cm^{-1} are assigned to the A_{1g} modes, which are the stretching modes of the anatase phase of the titania. It should be noted that the frequency of the 144 cm^{-1} band is very intense and sharp and is nearly equal to that of the rutile phase, which is at 143 cm^{-1}. However, the difference is that the rutile phase band is sharp but weak (Ohsaka et al. 1978; Lei et al. 2001). This is important because it confirms that doping the TiO$_2$ with metal ions does not alter the phase, which is a very important feature when studying the degradation of organic pollutants by photo active semi-conductors.

The Raman peaks associated with both the anatase phase and the CCA modes both appear in the graph of the TiO$_2$ supports. This is an indication that the impregnation of the CCA supports by the TiO$_2$ was successful. However, the intensities of the peaks associated with the titania show that TiO$_2$ might be suppressed. This could be due to the surface modification of titania by the presence of carbon. Carbon can easily disperse on the surface of titania, a special property that might result in an improved catalytic activity of the titania (Lin et al. 2005a, b).
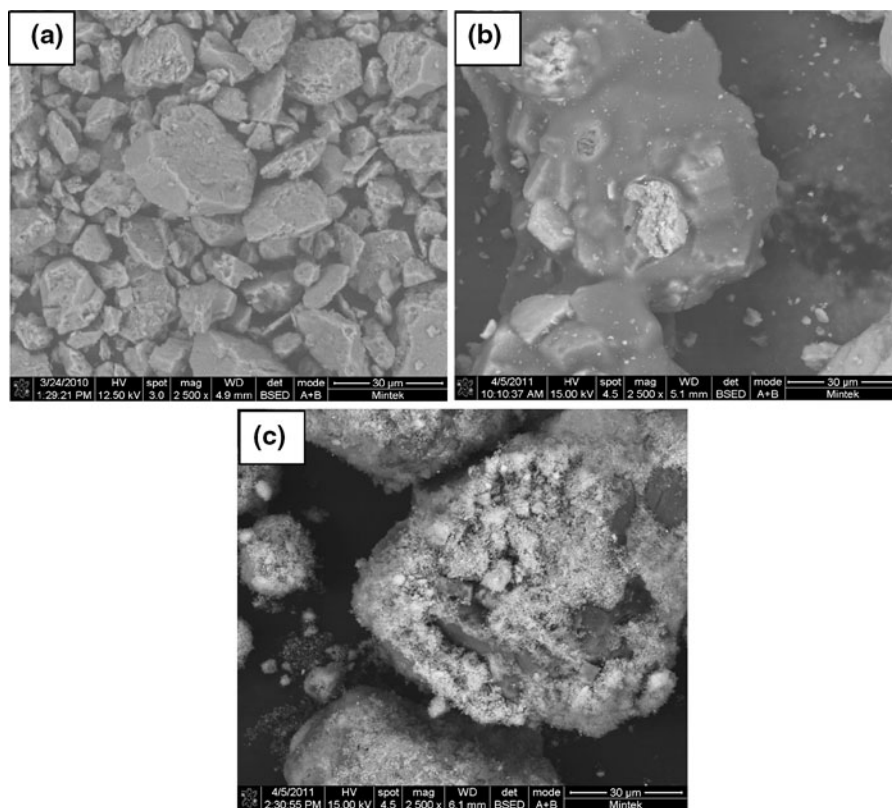

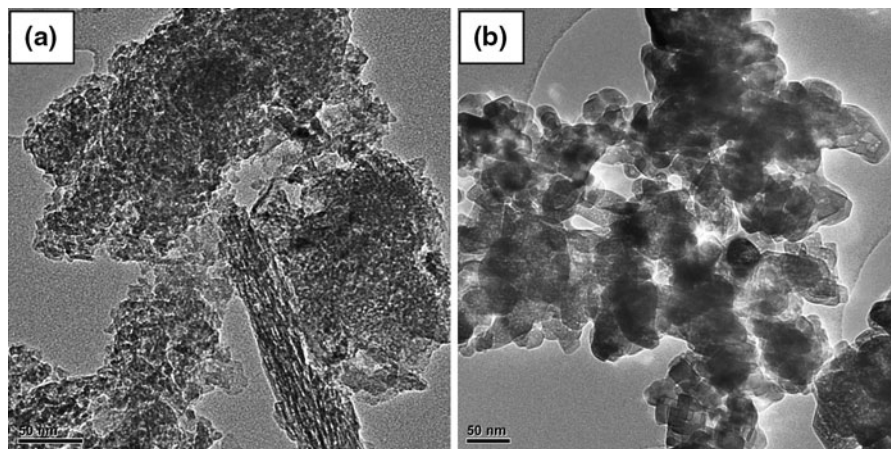**Fig. 3** SEM micrographs of **a** alumina, **b** CCA and **c** CCA-TiO$_2$

Fig. 4 TEM micrographs of alumina (**a**), CCA (**b**) and CCA-TiO$_2$

SEM, TEM and EDX spectroscopy

The SEM micrographs (Fig. 3) show the physical morphology of the alumina (a), CCA (b) and CCA-TiO$_2$ (c). The SEM micrographs show that a carbon layer has been deposited on the alumina support. The carbon layer appears to be homogeneously distributed on the surface of the alumina. Also, the alumina and CCA support surfaces appear to be porous and hence provide a large surface area for use as catalysts supports. Fig. 3c shows the TiO$_2$ nanocatalysts that are embedded on the CCA support surface. The titania nanocatalysts appear embedded on the pores of the CCA supports, hence giving the idea that they can be used in catalysis without falling away from the supports. Figure 4 shows TEM micrographs of the CCA supports (a) and the TiO$_2$ embedded supports (b). The CCA supports appear microporous and fluffy, an effect of carbon coating. Figure 4b shows the TEM micrograph of the TiO$_2$ embedded supports. The supported titania catalysts still appear to have not lost their crystallinity, and hence the assumption that the catalytic activity of the catalysts has not been altered, but an improvement might be expected. To identify the elemental composition of the synthesized catalyst and supports, the EDX spectra for the alumina (Fig. 5a), CCA (Fig. 5b) and CCA-TiO$_2$ (Fig. 5c) were also studied. These showed that the alumina was composed of only Al and O, while the CCA has C as an extra element. The CCA-TiO$_2$ spectrum shows the presence of Al, O, C and Ti. The EDX

spectra therefore not only indicate the successful incorporation of carbon on the surface of alumina but also the successful impregnation of the CCA with the TiO$_2$ nanocatalysts.

BET surface area and pore size distribution measurements

The nitrogen adsorption–desorption isotherms were measured to understand the influence of carbon loading on the surface of the alumina as well as the effect of embedding the TiO$_2$ nanocatalysts on the CCA (Figs. 6, 7, 8). Figure 6 shows the adsorption–desorption isotherm of γ-alumina and the insert graph shows the pore size distribution graphs of the γ-alumina. Figure 7 shows the adsorption–desorption isotherm of the CCA support with the pore size distribution graph shown as an insert and Fig. 8 shows the adsorption–desorption isotherm of CCA-TiO$_2$ with the insert showing the pore size distribution graph. According to the Brunauer–Emmett–Teller (BET) classification, these adsorption–desorption isotherms can be classified as type IV. This type of isotherm describes the process of nitrogen adsorption on the adsorbent surface. Pure alumina, CCA and CCA-TiO$_2$ were all found to possess a heterogeneous pore structure. These microporous pores were filled up with the adsorbate (nitrogen) at small pressures and as the adsorbate concentration increases, pores of larger diameters were also filled up resulting in the formation of a multimolecular adsorption layer. Evidence of the occurrence of open pores in the alumina, CCA

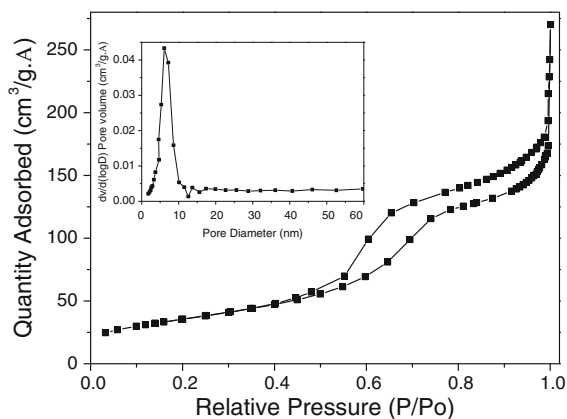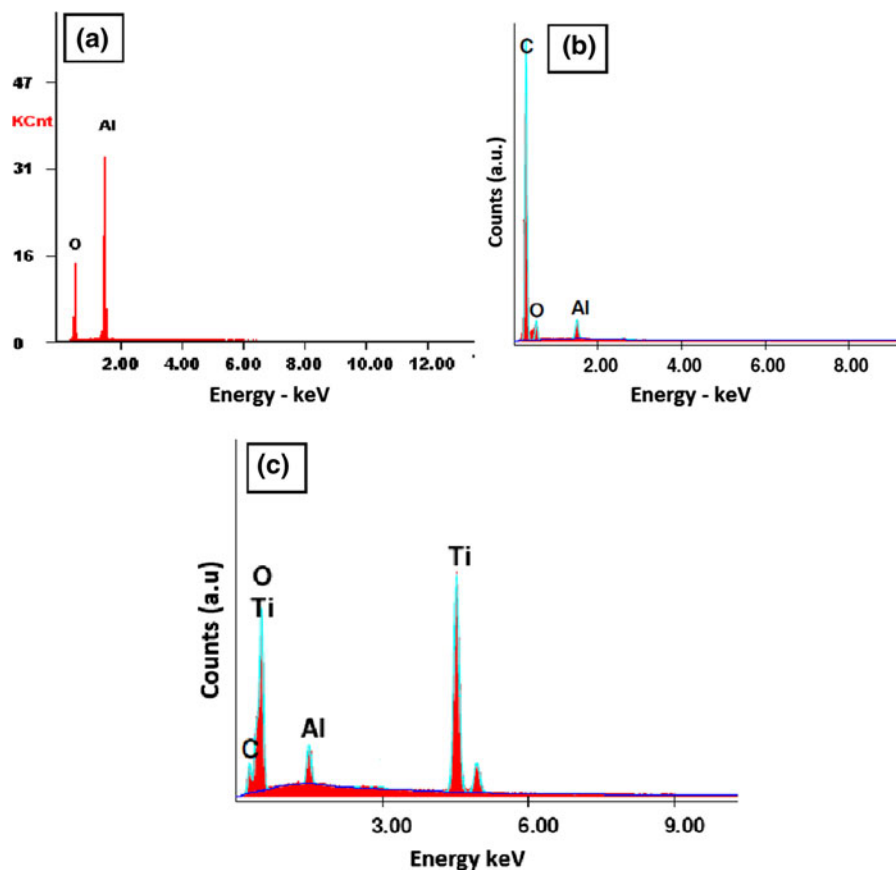**Fig. 5** EDX spectra of **a** alumina and **b** CCA and **c** CCA-TiO$_2$

Fig. 6 Nitrogen adsorption–desorption isotherm of the initial alumina support

Fig. 7 Nitrogen adsorption–desorption isotherm of the CCA support

supports and CCA-TiO$_2$ are shown by the presence of the hysteresis loop in the diagrams.

To further study the texture and surface properties of alumina and the synthesized CCA supports, specific surface area, pore volume, pore size and pore size
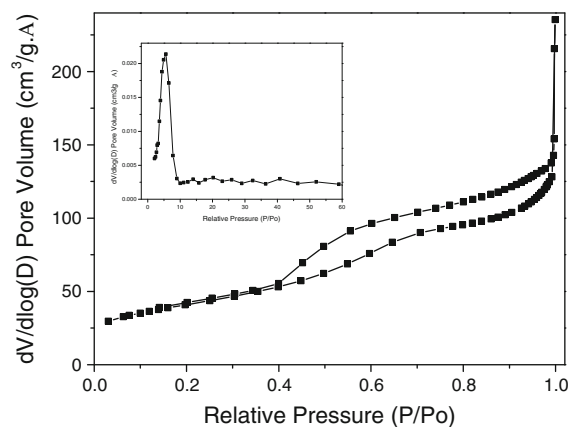
distribution were analysed according to the BJH method (insert graphs in Figs. 6, 7, 8) and are summarised in Table 1. The addition of the carbon layer on the surface of the alumina resulted in a significant increase in the surface area from
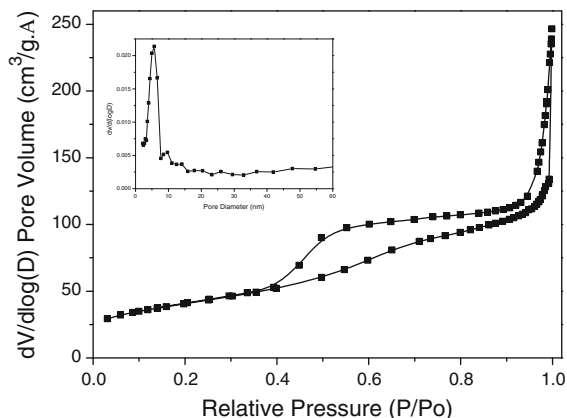
Fig. 8 Nitrogen adsorption–desorption isotherm of the CCA-TiO$_2$

Table 1 Textural properties of the CCA support

Sample	S_{BET} (N$_2$) (m^2 g^{-1})	Total pore volume (cm^3 g^{-1})	Mean pore diameter (nm)
Al$_2$O$_3$	128	0.27	8.36
CCA	146	0.20	5.41
CCA-TiO$_2$	149	0.21	5.69

128 m^2 g^{-1} (pure alumina), 146 m^2 g^{-1} (CCA) and 149 m^2 g^{-1} for the CCA-TiO$_2$. This increase is a result of the creation of new pore structures after the modification of the alumina surface (Błachnio et al. 2007). There is however a decrease on the pore volume (0.27–0.20 cm^3 g^{-1}) and mean diameter of the pores (8.36–5.41 nm) for the alumina and the CCA. This can be attributed to the formation of a uniform carbon layer on the alumina surface (Sharanda et al. 2006). This is an indication that carbon occupied the inner pores of the alumina, hence the decrease (Zheng et al. 2008). However, the addition of the nanocatalysts on the CCA resulted in no noticeable difference between the sizes of the pore volumes. A slight increase in diameter (from 5.41 to 5.69 nm) was observed for the CCA and CCA-TiO$_2$. Furthermore, the shape of the pore size distribution graphs fits a Gaussian curve distribution with peak maxima at 6.4 nm for alumina, 5.4 nm for the CCA support and 5.6 nm for the CCA-TiO$_2$.

Photodegradation of Rhodamine B

For the photodegradation studies, the dye was illuminated with visible light in the absence of the catalyst (photolysis) to determine the extent of degradation under visible light. This was done since rhodamine B has been reported to absorb light which is in the range of 400–600 nm (He et al. 2009; Natarajan et al. 2011). The reaction mixture was first stirred in the dark for 1 h to reach equilibrium between the catalyst and the dye before illumination with either the UV or visible light, and the concentration was monitored. It was found that there was only about 2% adsorption of the dye on the catalysts when the equilibrium was reached. Photodegradation of rhodamine B was tested using the free and CCA-supported titania catalysts both under UV light and visible light irradiation for comparison purposes.

The results obtained showed that photolysis had an average of about 4% degradation of Rhodamine B after about 4.5 h. As shown in Fig. 9, both the CCA-TiO$_2$ and the free titania nanocatalysts achieved complete degradation after 270 min. From these results, the CCA-TiO$_2$ nanocatalysts show a higher reaction rate than the free anatase titania. Unsupported titania could only degrade about 20% Rhodamine B under visible light illumination in 270 min compared to complete degradation under UV light irradiation. The results obtained (Fig. 9) also show that CCA-TiO$_2$ nanocatalysts were photocatalytically active under both visible and UV light, although it was more photocatalytically active under visible light. Under visible light irradiation the photodegradation of Rhodamine was complete within 180 min compared to about 240 min observed under UV light irradiation. Also, The CCA-supported TiO$_2$ nanocatalysts
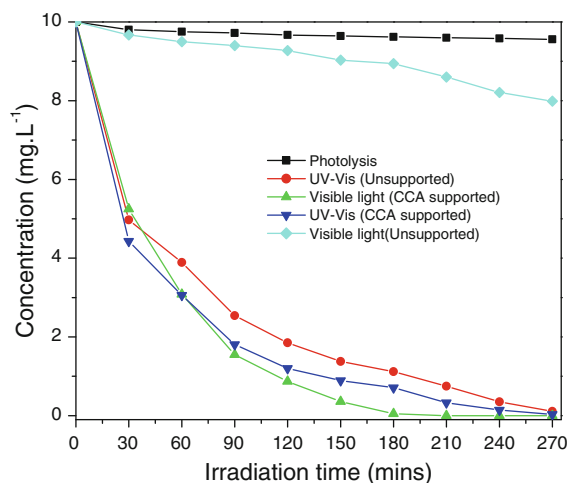

Fig. 9 Graph showing photodegradation of rhodamine B by free titania CCA-T under UV and visible light illumination

generally showed high photocatalytic activity than the unsupported titania nanocatalysts both under UV and visible light irradiation.

Conclusions

From this research study, the TiO_2 nanocatalysts were successfully embedded on CCA supports that were synthesized by exploiting the reactivity of the N=C=O groups of toluene 2,4 diisocyanate. The successful synthesis of the TiO_2 nanocatalysts-impregnated CCA supports was confirmed by UV Raman spectroscopy which showed the presence of the D and G olefinic carbon bands at 1318 and 1607 cm^{-1}, respectively, as well as the anatase TiO_2 peaks at 516 399, 639, 197 and 144 cm^{-1}. The SEM confirmed the presence of a uniform carbon layer on the surface of the alumina and the successful impregnation of the titania catalysts on the CCA supports. The EDX spectral analysis confirmed the elemental composition of the alumina, CCA supports as well as the CCA-TiO_2. Further analysis of the adsorption–desorption isotherms revealed that the presence of the carbon layer on the alumina surface resulted in an increase in surface area and a decrease in pore size and pore volume. This is a result of a formation of a uniform carbon layer on the alumina surface and also an indication that the carbon was modifying the pores of the alumina. However, although impregnating the supports with TiO_2 did result in an increase in surface area, there was no observable difference between the pore volume and pore diameter between the CCA supports and the CCA-TiO_2. Overall, for the first time the TiO_2 catalysts were successfully embedded on the CCA supports. The CCA-TiO2 nanocatalysts were found to be more photocatalytically active under visible light irradiation compared to their unsupported counterparts and this provides a great stride towards the use of the renewable solar energy for water treatment purposes.

References

Ahn W-Y, Sheeley SA, Rajh T, Cropek DM (2007) Photocatalytic reduction of 4-nitrophenol with arginine-modified titanium dioxide nanoparticles. Appl Catal B Environ 74:103–110. doi:10.1016/j.apcatb.2007.01.016

Anandan S, Kumar PS, Pugazhenthiran N, Madhavan J, Maruthamuthu P (2008) Effect of loaded silver nanoparticles on TiO_2 for photocatalytic degradation of Acid Red 88. Sol Energy Mater Sol Cells 92:929–937. doi:10.1016/j.solmat.2008.02.020

Ao Y, Xu J, Fu D, Yuan C (2008) Preparation of Ag-doped mesoporous titania and its enhanced photocatalytic activity under UV light irradiation. J Phys Chem Solids 69:2660–2664. doi:10.1016/j.jpcs.2008.06.100

Bessekhouad Y, Robert D, Weber JV (2003) Synthesis of photocatalytic TiO_2 nanoparticles: optimization of the preparation conditions. J Photochem Photobiol A Chem 157:47–53. doi:10.1016/s1010-6030(03)00077-7

Błachnio M, Staszczuk P, Grodzicka G, Lin L, Zhu YX (2007) Adsorption and porosity properties of carbon-covered alumina surfaces. J Therm Anal Calorim 88(2):601–606. doi:10.1007/s10973-006-8067-3

Boorman PM, Chong K (1992) A comparative gas oil hydroprocessing study of alumina, carbon, and carbon-covered alumina supported Ni–Mo catalyst: effect of quinoline, thiophene, and vanadium spiking. Energy Fuels 6:300–307. doi:10.1021/ef00033a10

Boorman P, Chong K (1993) Preparation of carbon-covered alumina using fluorohydrocarbons: a new acidic support material. Appl Catal A Gen 95:197–210. doi:10.1016/0926-860x(93)85074-y

Calandra P, Lombardo D, Pistone V, Liveri T, Trusso C (2010) Structural and optical properties of novel surfactant-coated Yb@TiO_2 nanoparticles. J Nanopart Res. doi:10.1007/s11051-010-0133-x

Chen X, Mao SS (2007) Titanium dioxide nanomaterials: synthesis, properties, modifications, and applications. Chem Rev 107:2891–2959. doi:10.1021/cr0500535

Colmenares JC, Aramendia MA, Marinas A, Marinas J, Urbano F (2006) Synthesis, characterization and photocatalytic activity of different metal-doped titania systems. Appl Catal A Gen 306:120–127. doi:10.1016/j.apcata.2006.03.046

Fang WQ, Zhou JZ, Liu J, Chen ZG, Yang C, Sun CH, Qian GR, Zou J, Qiao SZ (2011) Hierarchical structures of single-crystalline anatase TiO_2 nanosheets dominated by 001 facets. Chem Eur J 17:1423–1427. doi:10.1002/chem.201002582

Foglia FD, Losco T, Piseri P, Milani P, Selli E (2009) Photocatalytic activity of nanostructured TiO_2 films produced by supersonic cluster beam deposition. J Nanopart Res 11:1339–1348. doi:10.1007/s11051-009-9691-1

Foster HA, Ditta IB, Varghese S, Steele A (2011) Photocatalytic disinfection using titanium dioxide: spectrum and mechanism of antimicrobial activity. Appl Microbiol Biotechnol 90:1847–1868. doi:10.1007/s00253-011-3213-7

Fu W, Yang H, Li M, Li M, Yang N, Zou G (2005) Anatase TiO_2 nanolayer coating on cobalt ferrite nanoparticles for magnetic photocatalyst. Mater Lett 59:3530–3534. doi:10.1016/j.matlet.2005.06.071

He Z, Sun C, Yang S, Ding Y, He H, Wang Z (2009) Photocatalytic degradation of rhodamine B by Bi_2WO_6 with electron accepting agent under microwave irradiation: mechanism and pathway. J Hazard Mater 162:1477–1486. doi:10.1016/j.jhazmat.2008.06.047

Hoffmann MR, Martin ST, Choi W, Bahnemannt DW (1995) Environmental applications of semiconductor photocatalysis. Chem Rev 95:69–96. doi:10.1016/j.ces.2007.06.030

Jana P, Ganesan V (2011) The production of a carbon-coated alumina foam. Carbon 49:3292–3298. doi:10.1016/j.carbon.2011.04.005

Lei Y, Zhang LD, Fan JC (2001) Fabrication, characterization and Raman study of TiO$_2$ nanowire arrays prepared by anodic oxidative hydrolysis of TiCl$_3$. Chem Phys Lett 338:231–236. doi:10.1021/s0009-2614(01)00263-9

Li X, Xiong R, Wei G (2008) S–N Co-doped TiO$_2$ photocatalysts with visible-light activity prepared by sol–gel method. Catal Lett 125:104–109. doi:10.1007/s10562-008-9521-6

Lin L, Lin W, Zhu YX, Zhao BY, Xie YC, He Y, Zhu YF (2005a) Uniform carbon-covered titania and its photocatalytic property. J Mol Catal 236:46–53. doi:10.1016/j.molcata.2005.04.028

Lin L, Lin W, Zhu YX, Zhao BY, Xie YC, Jia GQ, Li C (2005b) Uniformly carbon-covered alumina and its surface characteristics. Langmuir 21(11):5040–5046. doi:10.1021/la047097d

Maity SK, Flores L, Ancheyta J, Fukuyama H (2009) Carbon-modified alumina and alumina-carbon supported hydrotreating catalysts. Ind Eng Chem Res 48:1190–1195. doi:10.1021/ie800606p

Mori K, Maki K, Kawasaki S, Yuan S, Yamashita H (2008) Hydrothermal synthesis of TiO$_2$ photocatalysts in the presence of NH$_4$F and their application for degradation of organic compounds. Chem Eng Sci 63:5066–5070. doi:10.1016/j.ces.2007.06.030

Natarajan TS, Thomas M, Natarajan K, Bajaj HC, Tayade RJ (2011) Study on UV-LED/TiO$_2$ process for degradation of Rhodamine B dye. Chem Eng J 169:126–134. doi:10.1016/j.cej.2011.02.066

Navio JA, Colon G, Macias M, Real C, Litter MI (1999) Iron-doped titania semiconductor powders prepared by a sol-gel method. Part I: synthesis and characterization. Appl Catal A Gen 177:111–120. doi:10.1016/s0926-860x(98)00255-5

Ohsaka T, Izumi F, Fujiki Y (1978) Raman spectrum of anatase TiO$_2$. J Raman Spectrosc 7(6):321–324. doi:10.1002/jrs.1250070605

Paek C, Mccormick AV, Carr PW (2010) Preparation and evaluation of carbon coated alumina as a high surface area packing material for high performance liquid chromatography. J Chromatogr A 1217:6475–6483. doi:10.1016/j.chroma.2010.08.037

Polyánszky É, Petró J (1990) Relationship between selectivity and hydrogen sorption of carbon-supported palladium catalysts. Appl Catal 62:335–347. doi:10.1016/s0166-9834(00)82256-3

Rao KSR, Rao PK, Masthan SK, Kaluschnaya L, Shur VB (1990) New type of carbon coated alumina supports for the preparation of highly active ruthenium catalysts for ammonia synthesis. Appl Catal 62:L19–L22. doi:10.1016/s0166-9834(00)82229-0

Sharanda LF, Plyuto YV, Babich IV, Plyuto IV, Shpak AP, Stoch J, Moulijn JA (2006) Synthesis and characterisation of hybrid carbon-alumina support. Appl Surf Sci 252:8549–8556. doi:10.1016/j.apsusc.2005.11.078

Shashikala V, Kumar VS, Padmasri AH, Raju BD, Mohan SV, Sarma KS, Rao KSR (2007) Advantages of nano-silver-carbon covered alumina catalyst prepared by electro-chemical method for drinking water purification. J Mol Catal A Chem 268:95–100. doi:10.1016/j.molcata.2006.10.019

Tian G, Fu H, Jing L, Tian C (2009) Synthesis and photocatalytic activity of stable nanocrystalline TiO$_2$ with high crystallinity and large surface area. J Hazard Mater 161:1122–1130. doi:10.1016/j.jhazmat.2008.04.065

Ulgen A, Hoelderich WF (2011) Conversion of glycerol to acrolein in the presence of WO$_3$/TiO$_2$ catalysts. Appl Catal A Gen 400:34–38. doi:10.1016/j.apcata.2011.04.005

Vissers J, Mercx F, Bouwens S, de Beer V, Prins R (1988) Carbon-covered alumina as a support for sulfide catalysts. J Catal 114:291–302. doi:10.1016/0021-9517(88)90033-4

Wang J, Li R, Zhang Z (2008) Degradation of hazardous dyes in wastewater using nanometer mixed crystal TiO$_2$ powders under visible light irradiation. Water Air Soil Pollut 189:225–237. doi:10.1007/s11270-007-9570-2

Yu J, Zhang J (2010) A simple template-free approach to TiO$_2$ hollow spheres with enhanced photocatalytic activity. Dalton Trans 39:5860–5867. doi:10.1039/c0dr00053a

Yu JC, Lin J, Kwok RWM (1997) Enhanced photocatalytic activity of Ti$_{1-x}$V$_x$O$_2$ solid solution on the degradation of acetone. J Photochem Photobiol A Chem 111:199–201. doi:1010-6030(97)00207-4

Zheng M, Shu Y, Sun J, Zhang T (2008) Carbon-covered alumina: a superior support of noble metal-like catalysts for hydrazine decomposition. Catal Lett 121:90–96. doi:10.1007/s10562-007-9300-9

Zhu J, Zhang J, Chen F, Iino K, Anpo M (2005) High activity TiO$_2$ photocatalysts prepared by a modified sol–gel method: characterization and their photocatalytic activity for the degradation of XRG and X-GL. Top Catal 35(3–4):261–268. doi:10.1007/s11244-005-3833-1

Zhu J, Yang D, Geng J, Chen D, Jiang Z (2008) Synthesis and characterization of bamboo-like CdS/TiO$_2$ nanotubes composites with enhanced visible-light photocatalytic activity. J Nanopart Res 10:729–736. doi:10.1007/s11051-0007-9301-z